Dynamic Testbed Demonstration of WFIRST Coronagraph Low Order Wavefront Sensing and Control (LOWFS/C)

Fang Shi, Eric Cady, Byoung-Joon Seo, Xin An, Kunjithapatham Balasubramanian, Brian Kern, Raymond Lam, David Marx, Dwight Moody, Camilo Mejia Prada, Keith Patterson, Ilya Poberezhskiy, Joel Shields, Erkin Sidick, Hong Tang, John Trauger, Tuan Truong, Victor White, Daniel Wilson, and Hanying Zhou
Jet Propulsion Laboratory, California Institute of Technology
4800 Oak Grove Drive, Pasadena, USA, CA 91009, USA

ABSTRACT

To maintain the required performance of WFIRST Coronagraph in a realistic space environment, a Low Order Wavefront Sensing and Control (LOWFS/C) subsystem is necessary. The LOWFS/C uses a Zernike wavefront sensor (ZWFS) with the phase shifting disk combined with the starlight rejecting occulting mask. For wavefront error corrections, WFIRST LOWFS/C uses a fast steering mirror (FSM) for line-of-sight (LoS) correction, a focusing mirror for focus drift correction, and one of the two deformable mirrors (DM) for other low order wavefront error (WFE) correction. As a part of technology development and demonstration for WFIRST Coronagraph, a dedicated Occulting Mask Coronagraph (OMC) testbed has been built and commissioned. With its configuration similar to the WFIRST flight coronagraph instrument the OMC testbed consists of two coronagraph modes, Shaped Pupil Coronagraph (SPC) and Hybrid Lyot Coronagraph (HLC), a low order wavefront sensor (LOWFS), and an optical telescope assembly (OTA) simulator which can generate realistic LoS drift and jitter as well as low order wavefront error that would be induced by the WFIRST telescope's vibration and thermal changes. In this paper, we will introduce the concept of WFIRST LOWFS/C, describe the OMC testbed, and present the testbed results of LOWFS sensor performance. We will also present our recent results from the dynamic coronagraph tests in which we have demonstrated of using LOWFS/C to maintain the coronagraph contrast with the presence of WFIRST-like line-of-sight and low order wavefront disturbances.

Keywords: WFIRST Coronagraph, Exoplanet, wavefront sensing and control, low order wavefront sensor, high contrast imaging, Zernike wavefront sensor, fast steering mirror, deformable mirror

1 LOW ORDER WAVEFRONT SENSING AND CONTROL FOR WFIRST CORONAGRAPH INSTRUMENT

1.1 Disturbances for WFIRST coronagraph instrument

Wide-Field InfraRed Survey Telescope (WFIRST) mission includes the first high contrast stellar coronagraph in space intended for imaging, discovery, and spectral characterization of Jupiter, Neptune, and possibly super-Earth sized exoplanets, as well as debris discs. The WFIRST Coronagraph Instrument (CGI) consists of two coronagraph modes: Hybrid Lyot Coronagraph (HLC) and Shaped Pupil Coronagraph (SPC) with each configuration has its unique and complimentary science role and capability [1]. The WFIRST CGI uses the active wavefront sensing and control to suppress the starlight and has an imaging camera and integral field spectrograph (IFS) working in visible band [2, 3].

One of the challenges to the coronagraph performance comes from the tight requirement on the WFIRST CGI optical wavefront stability necessary to achieve the required level of starlight suppression and the stability of coronagraph contrast. The wavefront dynamics presented to the coronagraph consists of wavefront errors (WFE) in both the line-of-sight (wavefront tilt) and low order wavefront aberrations such as focus, astigmatism, and coma. Depending on the sources of disturbances, these wavefront errors contain both low and high temporal frequency components, with the low frequency (sub Hz) WFE coming mostly from thermal load variation, and high frequency WFE from the vibration disturbances such as the reaction wheel assemblies (RWA) used for WFIRST telescope pointing.

The slow (< 2 Hz) LoS drift is from the telescope's attitude control system (ACS) residual pointing error. The WFIRST ACS requirement allows the telescope pointing error up to 14 milli-arcsec rms (mas) per axis. The fast LoS jitter is caused by vibrations from the ACS's reaction wheels assemblies (RWA). During the coronagraph observations, the RAW wheel speed varies slowly, typically ramping up from 10 rev/sec to 40 rev/sec in 18 hours. Because the slow variation of RWA speed, the LoS jitter is tonal with fundamental frequency corresponding to the RWA's wheel speed. While the most of LoS jitter energy contains at the fundamental frequency, the LoS jitter does have multiple harmonic and sub-harmonic frequencies. WFIRST observatory requirement allows LoS jitter up to 14 mas per axis.

During the coronagraph science observation, the spacecraft orbiting or telescope pointing will change the solar thermal load on the observatory, which will in turn cause the telescope's optics relative positions or surface figures to change. The integrated modeling of the WFIRST has shown that the thermally induced wavefront drift is about 0.5 nm rms. The dominant portion of the WFE are focus, astigmatisms, and comas, caused by the telescope's optics position shifts from the thermal load variations. Higher aberration modes beyond spherical are all negligibly small, in single digit picometer. It is also evident that the wavefront drifts are very slow, typically under 0.001 Hz.

1.2 LOWFS/C for WFIRST Coronagraph

A high contrast coronagraph instrument is very sensitive to the wavefront error [4, 5]. For WFIRST Coronagraph the science requires the coronagraph to have raw contrast better than 10^{-8}. Additionally, in order to differentiate planets from residual speckles in the dark hole and to measure the planet with a proper signal-to-noise ratio, the coronagraph contrast needs to be stable at a level of a few $\times 10^{-10}$ during the observation. The contrast stability requirement drives a very tight tolerance for the wavefront error and line-of-sight jitter. For example, for the sensitive WFE modes, such as spherical, coma, and trefoil, they need to be stable at 10s of picometer to maintain the contrast stability of $\sim 10^{-10}$. In order to maintain the coronagraph contrast level and stability WFIRST CGI needs a low order wavefront sensing and control (LOWFS/C) subsystem. From the coronagraph performance requirements, the WFIRST LOWFS/C's sensor needs to have the LoS sensitivity better than 0.4 mas and low order wavefront error sensitivity on the order of 10s of pm.

WFIRST Coronagraph LOWFS/C sensor uses the rejected starlight reflected off the coronagraph's focal plane occulting mask for wavefront sensing. Figure 1 shows the WFIRST CGI's optical function diagram including LOWFS/C. The LOWFS sensor is a Zernike wavefront sensor (ZWFS). One of the key features of WFIRST LOWFS/C design is that the Zernike wavefront sensor's phase shifting disk is designed and fabricated directly on the reflective side of the focal plane mask (FPM). In other words, the FPM has dual functions: coronagraph starlight suppression mask in transmission and LOWFS/C Zernike WFS mask in reflection. In this way, the starlight rejection and wavefront sensing occur at the same location. This not only ensures that the ZWFS measures WFE where the coronagraph needs but also avoids any significant non-common path error on ZWFS. The details of ZWFS mask design are different depending on the coronagraph mode [6, 7], but they all have the ZWFS phase shifting disk built in. For LOWFS/C the coronagraph's FPM acts as a low-pass spatial filter because of its limited size of the reflecting area, whose diameter is ~6 λ/D for HLC mask or ~5 λ/D for SPC mask. This low-pass filter nature causes the LOWFS/C Zernike wavefront sensor can only measure the low order wavefront error and is insensitive to mid and high spatial frequency WFE. Fortunately, the dominant WFIRST WFE drift and line-of-sight errors are low order in nature. The baseline WFIRST LOWFS/C ZWFS senses the first 11 low order Zernike terms: tilts (Z2, Z3), focus (Z4), astigmatisms (Z5, Z6), comas (Z7, Z8), trefoils (Z9, Z10), and spherical (Z11). A fixed 20% spectral filter centered at 550 nm is placed in front of the LOWFS/C camera. The baseline LOWFS/C camera uses the Teledyne E2V's EMCCD201, which will be modified for high frame rate of 1 KHz. The low order wavefront error, in the form of 10 Zernike coefficients (Z2-Z11), is computed at camera read out rate of 1 KHz.

The ZWFS sensed low order WFE is used to control corresponding wavefront correctors by the LOWFS/C, as shown in Figure 1. The sensed tip-tilt (Z2, Z3) is used to drive the Fast Steering Mirror (FSM) control loops at the command update rate of 1 KHz to suppress the LoS jitter and drift. Since the thermally induced WFE drift is very slow, the sensed low order WFE (Z4 – Z11) can be time-averaged over long period (minutes) to reduce the sensor noise without compromising the control bandwidth. The sensed focus term (Z4) is used to control the coronagraph's Focusing Mirror (FocM) which is an actuated fold flat mirror in a focused beam. Focus is the dominant mode of WFIRST WFE drifts so correcting it with the dedicated FocM will reduce the stroke burden on the deformable mirror. The rest of sensed low order wavefront error terms (Z5 – Z11), however, are used to drive DM1 for the correction.

In WFIRST Coronagraph, the role of LOWFS/C is to maintain the wavefront set by the HOWFS/C, which creates the coronagraph's dark hole at the beginning of a coronagraphic observation. The WFIRST LOWFS/C's sensor, therefore, works in the relative sensing mode, measuring the wavefront changes from the reference point set by HOWFS/C instead of measuring the absolute wavefront.

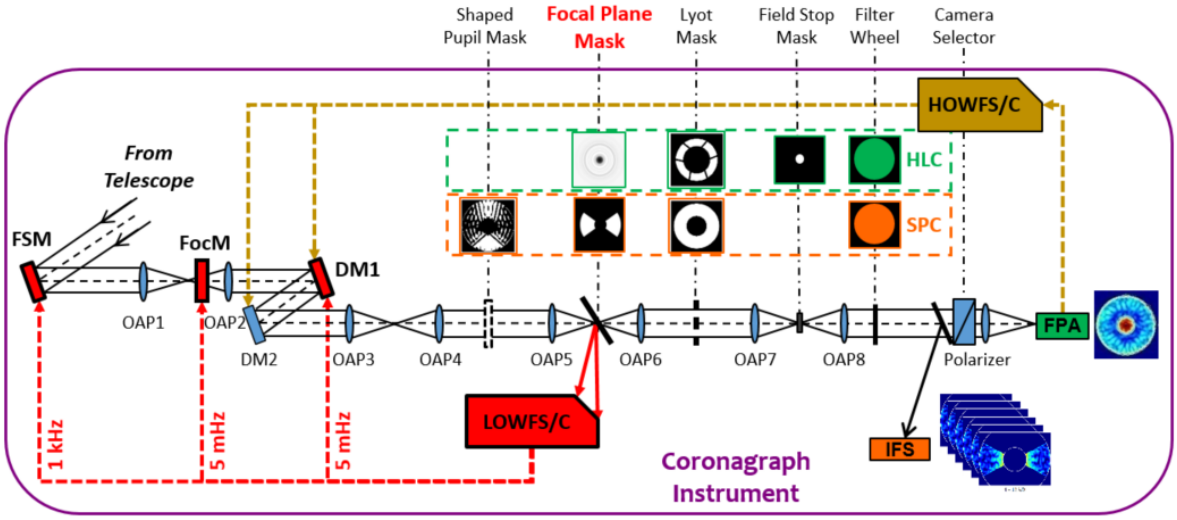

Figure 1. Functional illustration of WFIRST Coronagraph instrument (CGI) and LOWFS/C. Starlight from the telescope and relay optics enters CGI instrument at left through the fast steering mirror (FSM) at a pupil plane. Relay optics are off-axis parabolas (OAP) which form various image or pupil planes for coronagraph masks and stops. Two deformable mirrors (DM1 conjugated to pupil and DM2) are used by high order wavefront phase and amplitude control (HOWFS/C) to suppress the starlight for high contrast imaging. The WFIRST CGI can operate in either HLC or SPC mode. The Hybrid Lyot Coronagraph masks and stops (top row dashed box) and Shaped Pupil Coronagraph masks and stops (bottom row dashed box) are switched via filter wheel mechanisms (indicated by vertical dash lines) at corresponding pupil and image planes. A selectable mirror sends coronagraph light to either the imaging camera (FPA) or the integral field spectrograph (IFS). The rejected starlight reflected off the focal plane mask, which has the LOWFS/C phase dimple built-in, is captured by the LOWFS/C optics that form a pupil image on the LOWFS/C camera. The LOWFS/C subsystem controls FSM, Focusing Mirror (FocM), and DM1 with different updating frequencies as labeled in their corresponding control signal paths.

1.3 Zernike wavefront sensor concept

The Zernike wavefront sensor (ZWFS) is based on the Zernike phase-contrast concept [8, 9]. Figure 2 illustrates the concept of the Zernike wavefront sensor in the context of an astronomical instrument. The electric field at the entrance pupil is given by,

$$E(u,v) = P(u,v) \cdot A\big(1 + \varepsilon(u,v)\big) \cdot e^{i\varphi(u,v)} \approx P(u,v) \cdot A\big(1 + \varepsilon(u,v) + i\varphi(u,v)\big) \qquad (1)$$

where ***P(u,v)*** is the pupil amplitude support function, which describes the pupil geometry, ***A*** is the mean electric field amplitude, ***ε(u,v)*** is the amplitude variation across the entrance pupil, and ***φ(u,v)*** is the phase variation across the pupil, which is the wavefront error. The light from telescope is focused at an image plane, where a phase disk of size $\sim\lambda/D$ introduces a phase change of $\pi/2$ to the center potion of the PSF and forms a reference wavefront. The reference WF interferes with the light passing outside the phase disk which contains wavefront error. When imaged again to a pupil plane the interference turns the phase variation at the entrance pupil to the intensity variation in pupil image [10],

$$I(x,y) \approx A^2 \cdot \big(1 + \varepsilon^2(x,y) + 2\varphi(x,y)\big) \qquad (2)$$

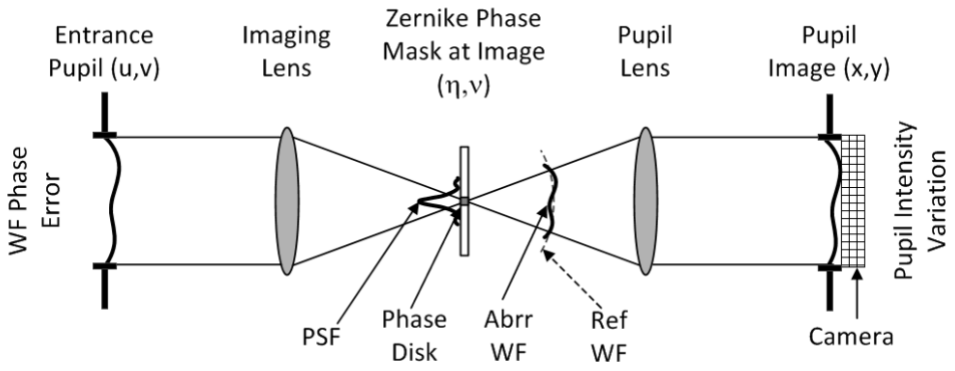

Figure 2. Illustration of Zernike wavefront sensor concept. Lenses are used to represent the optics between the entrance pupil, the imaging plane, and the re-imaged pupil plane. The Cartesian coordinates of these planes are also labeled.

Because ZWFS for WFIRST CGI is a relative wavefront sensor and the fact that the expected wavefront error during the WFIRST coronagraph observation is small, typically less than 1 nm RMS, we construct a differential image based linear algorithm to compute the relative wavefront error directly from the pupil image intensity. The differential images between the aberrated ZWFS image $\boldsymbol{I_{abbr}}$ and reference ZWFS image $\boldsymbol{I_{ref}}$ taken right after the HOWFS/C can then be used to derive the wavefront error changes $\boldsymbol{\Delta\varphi}$ needed for LOWFS/C,

$$\Delta\varphi = \left(\frac{I_{abbr} - I_{ref}}{2A^2}\right) = \frac{\Delta I}{2A^2} \tag{3}$$

More detailed mathematical description of Zernike wavefront sensor can be found in our JATIS paper [10]. In addition, extensive modeling and simulation have been carried out to evaluate the ZWFS performance for WFIRST CGI. The modeling results have shown that ZWFS can meet the WFIRST CGI requirements [10, 11].

1.4 The FSM line-of-sight control loop

The WFIRST LoS line-of-sight control loops are unique which worth some description here. Figure 3 shows the schematic overview of the WFIRST LOWFS/C line-of-sight control loops. The LoS control has two branches, a feedback loop and a feedforward loop [12]. The feedback control loop is shaped to reduce the sensor noise and provide control bandwidth to correct the slow LoS drift from ACS. The feedback loop also provides line-of-sight targets to allow LoS offset when the loop is closed. The feedforward loop uses the knowledge of RWA wheel speed from ACS telemetry and dynamic model identified harmonic frequencies together with LOWFS sensor to cancel the RWA wheel induced the LoS jitter. The feedforward loop uses recursive least mean squares (LMS) fitting of the tones to determine control signals directly fed to FSM to suppress tonal LoS jitter excited by the RWA [12, 13]. The error transfer function from the feedforward loop is notch filters at the controlled frequencies. To increase LMS robustness against the RWA wheel speed knowledge multiple ringers next to each other have been implemented to the feedforward loop.

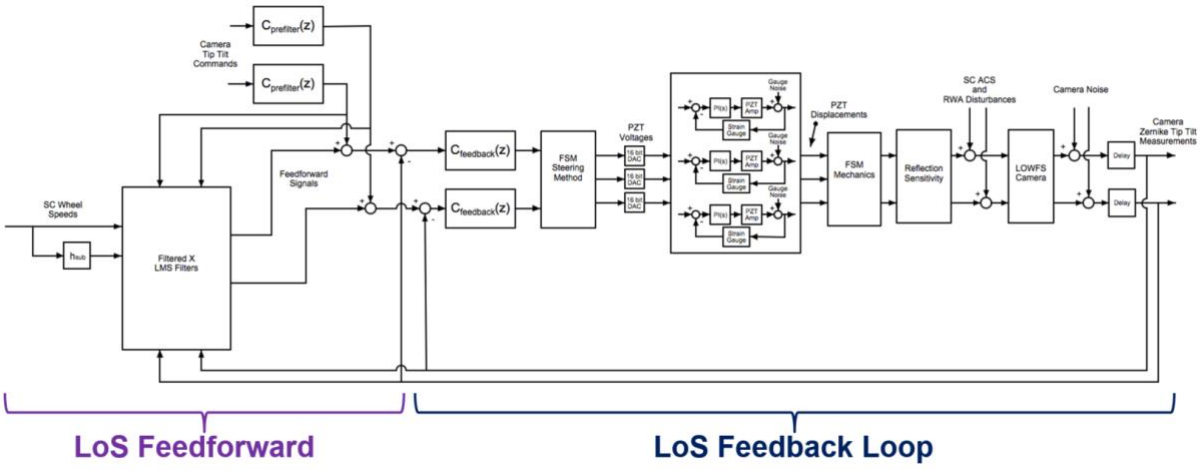

Figure 3. Block diagram depiction of the implemented line-of-sight drift and jitter compensation loops using a Fast Steering Mirror (FSM). The LoS control contains both the feedback loop and the feedforward loop. The control target inputs come in from the upper left and are filtered by $C_{prefilter}$. The ACS wheel speed input come from the left. The middle section is the FSM plant which has three PZT actuators and strain gauge local loops. The LOWFS camera and associated latency from frame grabber and computation are on the right. The WFE disturbances are introduced before the LOWFS camera.

The line-of-sight control uses the Fast Steering Mirror (FSM) with three PZT actuators and the design is inherited from the SIM project [13]. The FSM's PZT actuators have strain gauge sensors to close a local loop around the PZT displacements. This linearizes the hysteresis of the PZT and cancels any actuator drift or creep. To use the FSM for the feedforward control we need to have a good knowledge of the FSM transfer function. For the FSM used on testbed its tilt stroke, gain, linearity, and dynamic characteristics have been carefully measured and calibrated using various instruments such as Zygo, high-speed metrology system, and dynamometer [13]. These measurements and calibrations have been incorporated into the LoS control model.

2 OCCULTING MASK CORONAGRAPH TESTBED

Before integrated with the current dynamic testbed a dedicated LOWFS/C testbed including the OTA Simulator has been built and the stand-alone LOWFS/C tests have been carried out on this testbed in 2015 [14]. Using OTA Simulator to inject LoS drift and jitter, we have successfully demonstrated LOWFS/C LoS control with both feedback and feedforward loops. The LOWFS/C testbed has achieved loop control LoS error residuals to ~0.3 mas rms per axis for the favorable reaction wheel speeds that are typical in the planned RWA operational range, and to ~0.5 mas rms per axis for the worst-case RWA speeds and jitter values scaled to the requirements mentioned in Section 1.1. Furthermore, the test results have shown excellent agreement with the model predictions. However, the LOWFS/C testbed did not have a DM or SPC mask so the tests were limited to LoS control using a HLC mask and the FSM. More details of the LOWFS/C testbed descriptions and test results can be found in our previous 2016 SPIE paper [14].

In the parallel efforts, we have demonstrated the broadband coronagraph performance using two separated coronagraph testbeds, one for HLC and another for SPC. These coronagraph testbeds were static, without any disturbances injected and relying on passive isolation to keep out any lab environment [15, 16, and 17].

To demonstrate the coronagraph performance under the WFIRST like dynamic environment we have built the Occulting Mask Coronagraph (OMC) testbed. The OMC testbed mimics the WFIRST CGI design and has both HLC and SPC coronagraph modes, a LOWFS/C subsystem, and later on, an integral field spectrograph (IFS). It also an Optical Telescope Assembly (OTA) Simulator, which is directly carried over from the LOWFS/C testbed, for WFE disturbances injection.

Figure 4 shows the layout of the OMC testbed. The light starts at the OTA Simulator, which acts as the testbed's pseudo star, providing point source light with adjustable brightness and spectral bandwidth. It also creates the pupil with a shape that mimics the obscured 2.4-meter WFIRST telescope. The OTA Simulator also creates and injects the expected on-orbit WFIRST wavefront drift and LoS error into the testbed. The OTA Simulator relies on precise linear movement of the powered optics (miniature telescope, its secondary mirror, and OAP #2) to generate small (sub-nm) low order wavefront error modes such as focus, coma, astigmatism, and spherical aberration. To accurately move the powered optics we use PZT actuators with strain gauges that can provide microns of motion with sub nm precision and linearity better than 0.2%. The line-of-sight drift and jitter disturbances are generated by the Jitter Mirror (JM), which is located at a pupil plane and can run at speed up to 1 KHz.

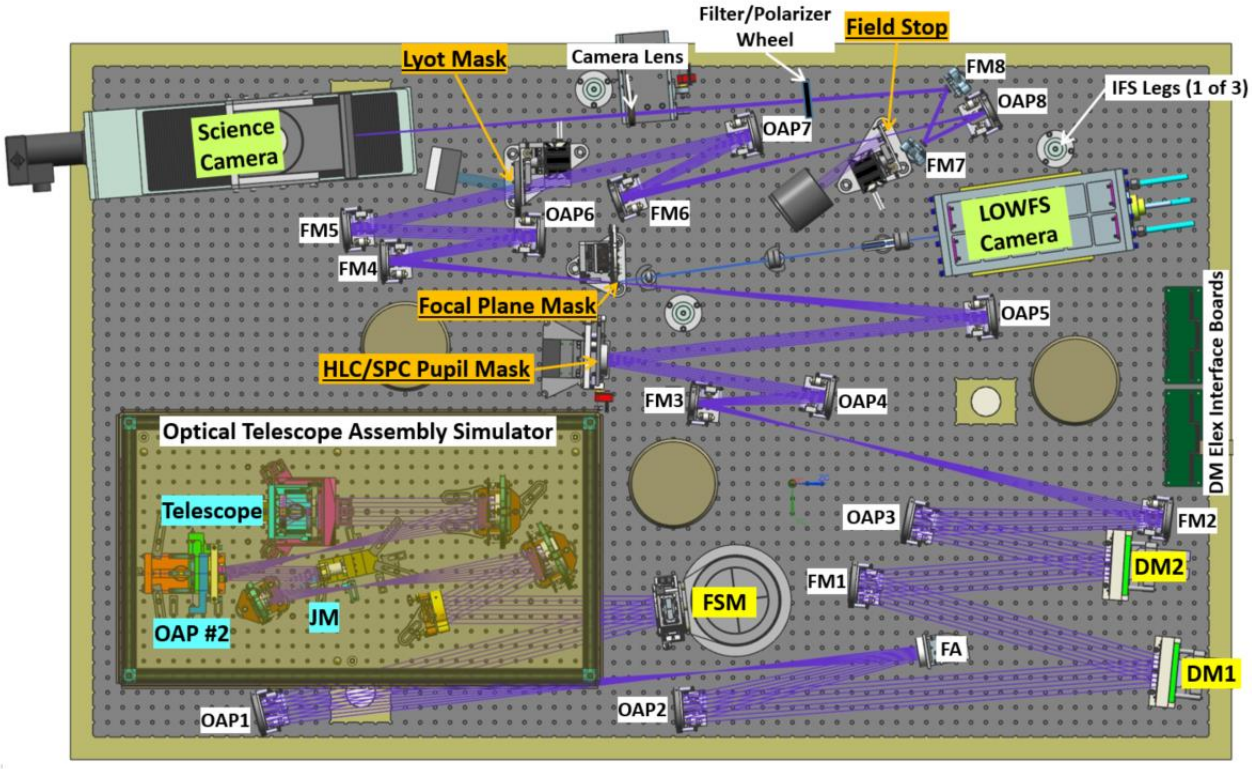

Figure 4. OMC testbed layout that shows the optical rays and opto-mechanical components on the optical table. The optical rays are from Zemax optical design. OTA Simulator sub-bench is at lower left. Light from a fiber fed pinhole acts as the pseudo star is collimated by the miniature telescope and masked by a WFIRST pupil mask. JM is used to generate line-of-sight disturbances and miniature telescope and OAP #2 are used to generate low order WFE. The disturbances generating optics are actuated by PZTs and their motions have been calibrated by Zygo. The output of the disturbed wavefront from OTA Simulator is coupled to the rest of coronagraph system at FSM, which is at one of the pupil planes. FSM, DM1 and DM2 are the active components on the testbed and they are used by HOWFS/C for starlight suppression and LOWFS/C for LoS and WFE disturbances suppression. Components with underlined labels are various coronagraph masks and stops for HLC and SPC. Off-axis parabola mirrors (OAP) and flat fold mirrors (FM) form various pupil and image planes for these masks and stops. Science Camera at upper left is used for high contrasting imaging HOWFS/C and coronagraph imaging. Rejected starlight from Focal Plane Mask reflects to the LOWFS optics which form a properly sampled pupil image on the LOWFS Camera.

One of the problems we have encountered with the OTA Simulator setup shown in Fig 4 is that the apparent size of the pseudo star from a 3 um pinhole was too large (~0.8 λ/D = 40 mas). In addition, the metallic commercial pinhole had some adverse wavefront impacts for coronagraph due to its waveguide effect. To improve the pseudo star quality we temporarily removed the miniature telescope and instead used a 60-inch OAP mirror to collimate the light from the pinhole. This has reduced apparent star size by about 5X. We also replaced the commercial metallic pinhole with

a thin Aluminum coated pinhole on a non-metallic substrate that was manufactured by JPL's Micro-device Lab (MDL). However, with this modification, we would rely on actuated linear stage to generate small focus to represent the low order WFE disturbances for the OMC testbed. This configuration was used for our coronagraph dynamic demonstration which results are presented in Section 3.3 later in this paper. In the future, we plan to reinstall the miniature telescope back to OTA Simulator bench and use a pair of OAPs to form a reduced pseudo star before the telescope. This will help us to regain the capability of generating other low order WFE modes besides focus. Figure 5 shows the current modifications of the OTA optics as well as an electron microscope image of the MDL pinhole.

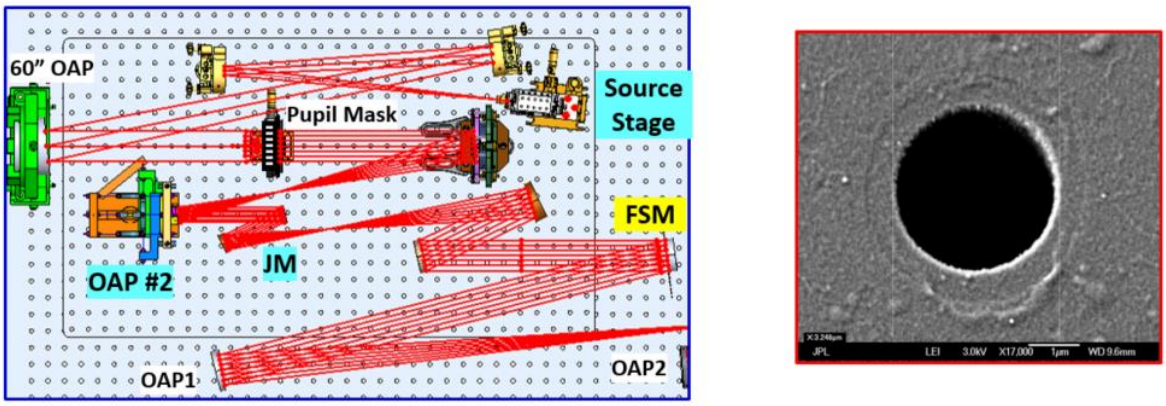

Figure 5. Modified OTA Simulator lay out on the left. The original OTA Simulator had the pseudo star pinhole at the focus of the miniature telescope. In this modified layout, the miniature telescope was taken out and replaced by the Pupil Mask that forms the WFIRST pupil for the testbed. The fiber pinhole assembly is mounted on an actuated stage which allows pinhole to translate in 3-axis for alignment purpose. A 60-inch OAP collimates the light from pinhole to illuminate the Pupil Mask and forms a ~5X smaller pseudo star for the testbed compared to that from the original miniature telescope. A pair of flat fold mirrors between the pinhole source and 60" OAP package the beam inside the OTA Simulator sub-bench. The light after the Pupil Mask follows the same path on OTA Simulator and the OMC testbed. The Z-axis motion of the source stage is used to generate focus aberration. The scale for the stage motion is 32 um source Z-motion create 1 nm rms focus (Z4). An etched pinhole on a non-metallic substrate made by JPL's MDL has replaced the commercial metallic pinhole. The image on the right is the electron microscope image of a 3 um pinhole which shows the MDL pinhole has a smooth edge and round shape formed on a thin (1 um thickness) membrane.

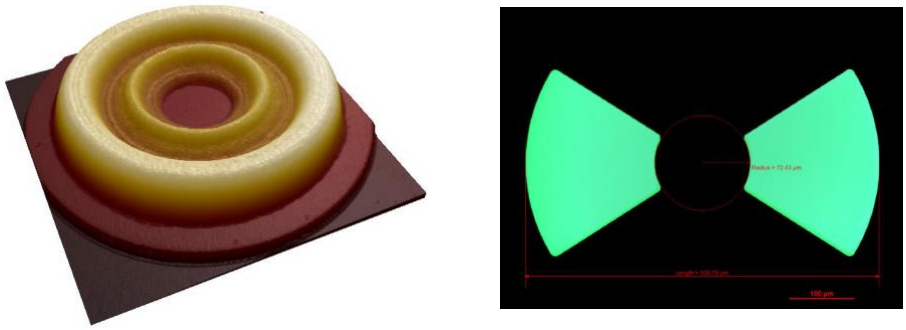

Figure 6. At left is the atomic force microscope scan of HLC focal plane mask that shows the dielectric profile. At right is the microscope image of the SPC focal plane mask. The green is transmissive region for SPC.

Figure 6 shows the focal plan masks (FPM) for HLC and SPC with ZWFS phase shifting disk built in. The ZWFS requires light within the phase dimple region has a $\pi/2$ radian phase difference from the outside region. For HLC

occulting mask this is done through the dielectric profile thickness change at the center λ/D region and for SPC bowtie mask this is achieved by etching down the center λ/D region of bowtie mask to create optical path delay directly.

Efforts have been made to isolate the testbed from the environmental disturbances in the lab. The OMC testbed is operated inside a vacuum chamber. The vacuum chamber and optical bench are thermally controlled. Mechanically the OMC optical bench sits on three Minus-K isolators with rigid body mode of only 0.5 Hz. Thermal sensor and accelerometer data are recorded and archived. The testbed can be operated remotely but also has a GUI for user to directly set up and change the hardware configurations on the testbed. The OMC testbed was build and integrated in 2015 and it was commissioned in early 2016. Characterizations, calibrations, and tests for coronagraph and LOWFS/C started immediately after the testbed commissioning.

3 OMC TESTBED RESULTS

We have conducted various tests on OMC testbed to evaluate and improve the performance of HLC and SPC coronagraphs and the LOWFS/C subsystem. This paper will concentrate on the performance results of the LOWFS/C. Results related to coronagraph high contrast imaging control and coronagraph performance can be found in papers of this conference by Byoung-Joon Seo, *et al*. for Hybrid Lyot Coronagraph [17] and by Eric Cady, *et al*. for Shaped Pupil Coronagraph [16].

3.1 Testbed results: LOWFS sensor accuracy and sensitivity

Tests have been carried out to understand LOWFS sensitivity and accuracy for tip-tilt and focus errors. The LOWFS sensed WFE is compared to the calibrated OTA Simulator input in order to characterize the sensor performance and determine the lowest wavefront error signal level that can be detected. To remove the effect from testbed drift, temporal square wave or sinusoidal modulated wavefront errors were used in the testbed to distinguish the injected disturbance from the lab environment noise and drift.

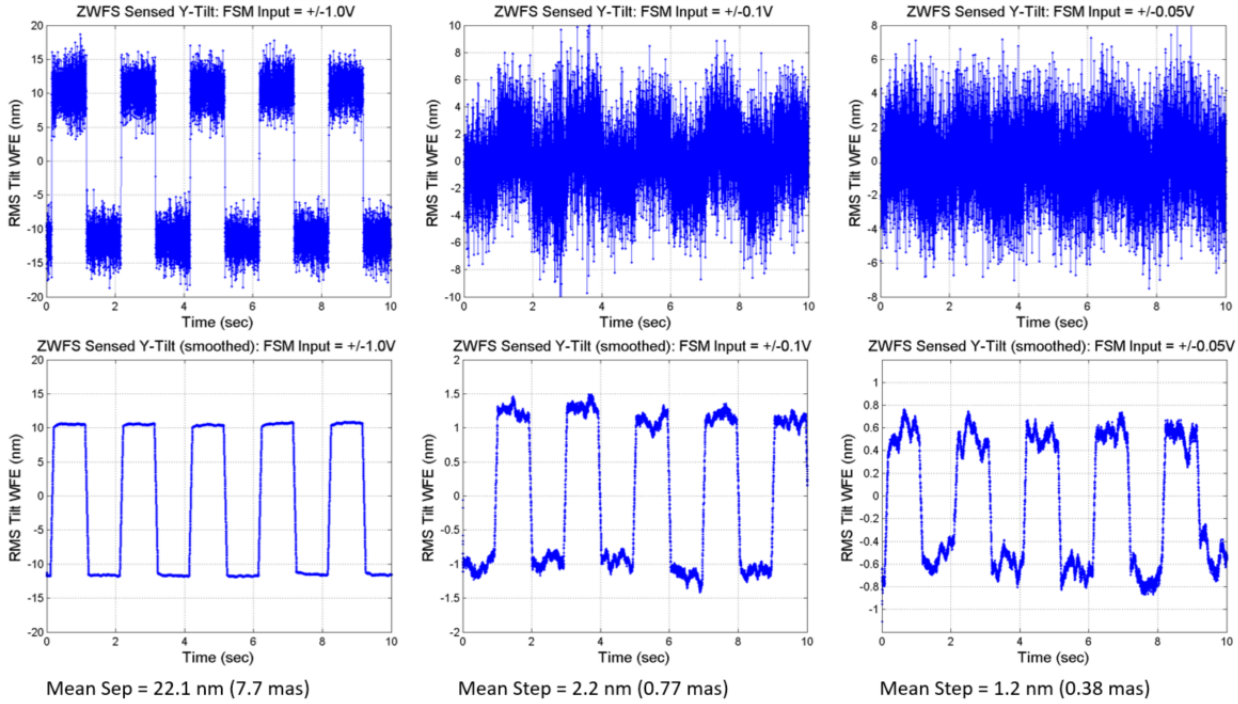

Figure 7. LOWFS sensing of injected tilts: raw data (top row) and smoothed data (bottom row). The injected input signal steps were: 22 nm (±3.9 mas on-sky equivalent) – left column; 2.2 nm (±0.39 mas on-sky equivalent) – middle column, and 1.1 nm (±0.19 mas on-sky equivalent) – right column. The plots shows the LOWFS sensed rms tilt wavefront error in nm.

Figure 7 shows results from LOWFS sensing small tilt disturbances. In this test the FSM, which has mirror tilt independently calibrated by a Zygo, is driven to introduce the tilt disturbances with various chopping step sizes. The figure plots both the noisier raw data acquired at 1 kHz rate and the smoothed data that reveal the modulated input tilt. When the detector noise is smoothed out the LOWFS sensor is clearly sensing the LoS chopping input as small as ±0.19 mas. Also shown in the plot, the sensed tilts match the input very well with sensing error less than 8% for the smallest input. Unfortunately, in this test we did not drive the FSM to amplitude smaller than ±0.19 mas.

Figure 8 shows the results from LOWFS sensing small focus disturbances. This test is done using the HLC occulting mask and the testbed DMs are set to flatten the wavefront. In this test the PZTs of OTA Simulator's telescope are driven with a sinusoidal signal that causes the distance between the telescope and pseudo star to vary, therefore introducing a sinusoidal modulation of focus (Z4) for the testbed. The OTA Simulator telescope PZTs have strain gauges to ensure their linearity and repeatability. The PZT and their induced focus have been independently calibrated using Zygo interferometer [14]. From plots in Figure 8 we can see that the LOWFS sensed focus matches the input very well and LOWFS can clearly sense focus as small as ±12 pm. However, due to the testbed drift, at the smallest amplitude (±12 pm) the LOWFS sensed focus has larger errors.

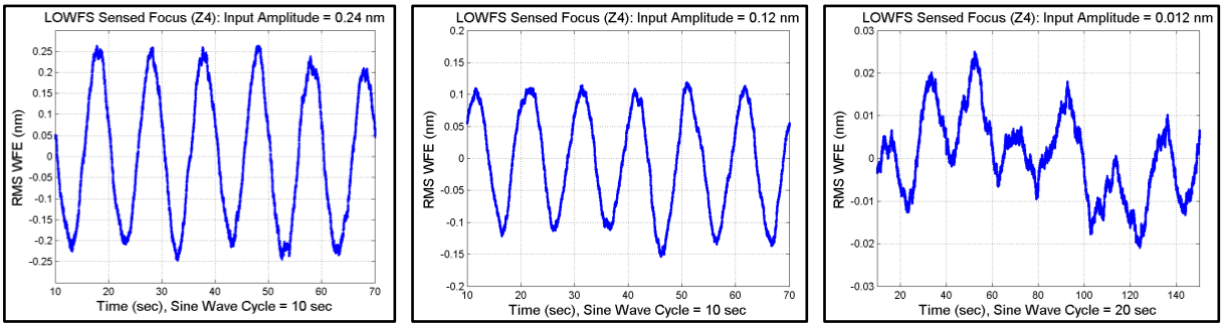

Figure 8. LOWFS sensing of injected focus (Z4). The plots show the LOWFS sensed focus vs time that corresponds to the sinusoidal input. From left to right the injected Z4 sinusoidal amplitude was ±0.24 nm, ±0.12 nm, and ±0.012 nm. The sinusoidal period are 10 sec for the left and middle plots and is increased to 20 sec for the 0.012 nm case. The longer period allows more averaging of the raw signals for noise reduction. LOWFS measures WFE at 500 Hz rate and the plots shows the boxcar smooth averaged data. From the left to the right plots the averaging boxcar size are: 1 sec, 2 sec, and 10 sec correspondingly.

3.2 Testbed results: comparing testbed data with model prediction

During the LoS testbed test the LoS disturbance from WFIRST Cycle 5 modeling was injected by the Jitter Mirror (for example, 14 mas LoS drift and LoS jitter at worst wheel speed of 600 rpm.) With both feedback and feedforward loops on the LOWFS/C was able to suppress the LoS error to below 0.5 mas per axis after the high frequency lab environment noises have been removed. The LoS closed loop performance has achieved for both HLC and SPC modes. Figure 9 compares testbed HLC data and predictions from the testbed LoS control model. The testbed LoS control model includes FSM metrology dynamic calibrations, testbed FSM and JM to LOWFS calibrations, measured LOWFS camera sensor noise, and LoS disturbance inputs injected by OAT Simulator's JM. The PSD plot on the left of Figure 9 shows that, except for the excess lab environment noises which was not included in the testbed model, the testbed data matches well to the testbed control model in both open and closed loop. The LoS error transfer function (ETF) plotted on the right is reflecting this excellent agreement.

As discussed in Section 1.1, the thermally induced low order wavefront drift for WFIRST CGI is very slow. To simulate it on testbed, we use the OTA Simulator to inject slow varying sinusoidal focus error to mimic the low order wavefront disturbances. The disturbances period varies from 90 min to 4 min (0.0002 Hz to 0.004 Hz). The testbed DM correction loop is a simple integrator with the closed-loop bandwidth about 0.03 Hz. Figure 10 shows the LOWFS/C's focus error transfer function for the DM correction loop, comparing the testbed data to the model prediction. Similar to the FSM control model the DM control model includes LOWFS sensor noise, sensor averaging time, DM to sensor calibration, and DM driver latency. The plot shows that the testbed data match the model very well. Surrounding the ETF plots are three focus residual vs. time plots for the three HLC test data points and they show that, as predicted by the modeled ETF, when the frequency of the disturbances decreases the DM loop has better focus suppression.

LOWFS/C has successfully closed line-of-sight loops using the FSM and low order WFE correction loop using one of the DMs on the OMC testbed for both HLC and SPC modes. The excellent agreement of control model and testbed data shown Figure 9 and Figure 10 have validated the control algorithms for LoS and low order WFE. A good model matching is very important for WFIRST because we rely on models to predict LOWFS/C's performance for flight instrument. As the testbed being update the testbed control models will be updated to reflect the changes of the testbed.

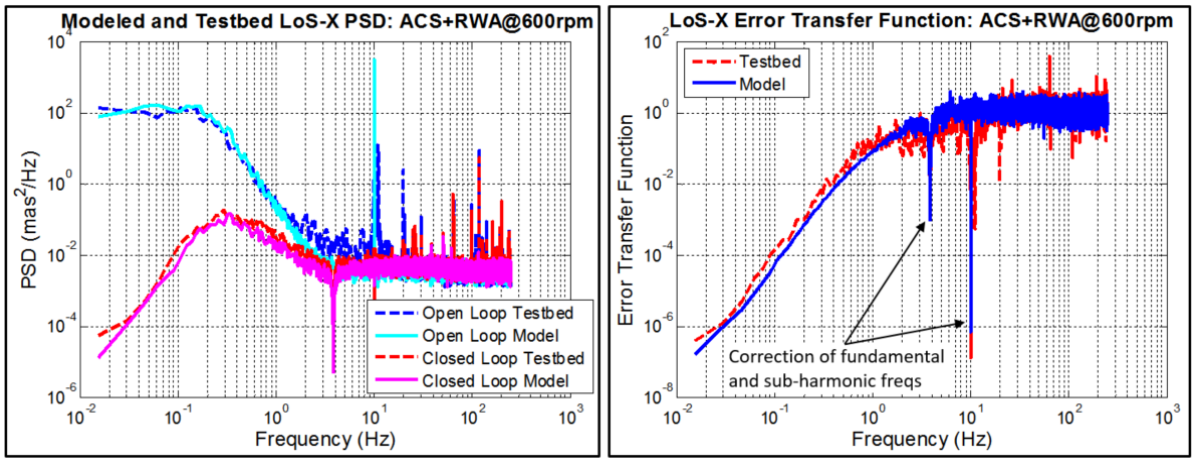

Figure 9. Compare testbed data (HLC) and testbed LoS control model. For plot clarity, we have only plotted data from X-axis. The plots on the left show the LoS power spectral density (PSD) of the open and closed loops. The LoS disturbances injected, which contain low frequency LoS drift and RWA induced tonal jitter with wheel speed of 600 rpm (10 Hz), are shown in the open-loop curves (blue dashed line – testbed data, cyan solid line – model). The excessive lab environment noises can be seen in the testbed data. The closed loop curves (red dashed line - testbed data, magenta solid line– model) show the correction from LoS feedback loop and feedforward loop acting on fundamental and sub-harmonic frequencies. The LoS loops are not designed to correct the lab environment noise shown as the spikes at higher frequencies. The plots on the right show the derived LoS closed-loop error transfer function (ETF). They are calculated as the ratio between closed-loop and open-loop data shown on the left plot. The ETF curves show the loops' suppression of low frequencies from the feedback loop and tonal notches at the fundamental and sub-harmonics.

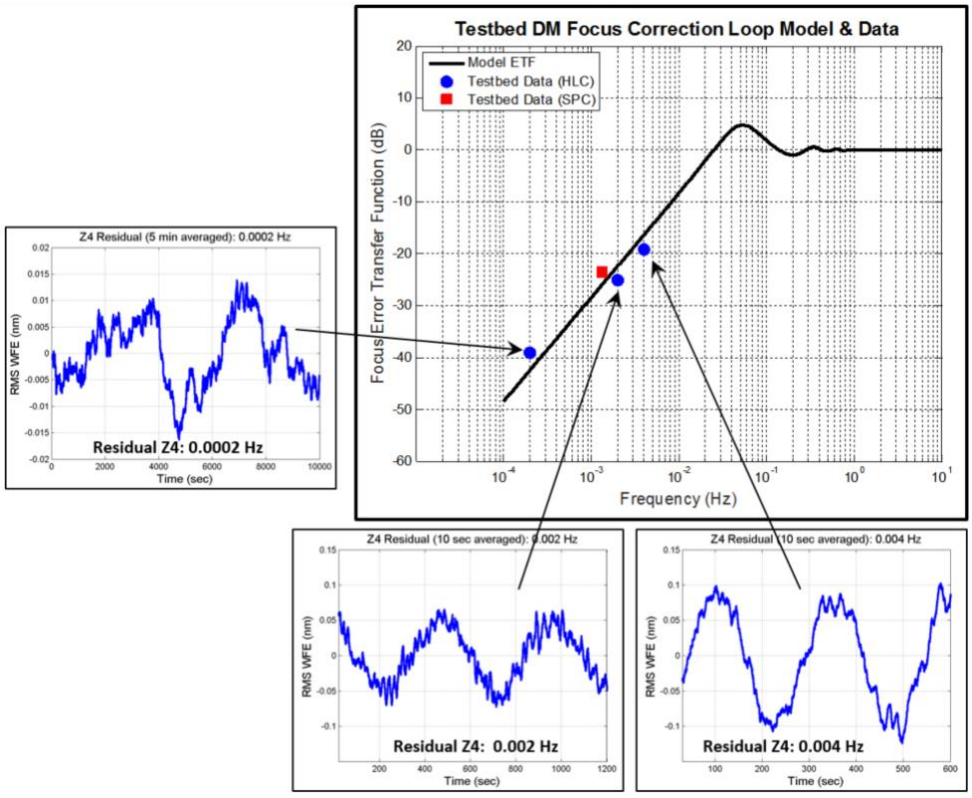

Figure 10. Testbed DM focus correction closed-loop error transfer function. The black line in the larger plot at upper right is the DM control model predicted ETF and the dots are the testbed LOWFS data from HLC (blue circle dot) and SPC (red square dot). Three small plots surrounding the ETF plots show the time traces of the post DM correction residual focus (Z4) corresponding to the three HLC testbed data. The frequencies of the sinusoidal input focus for these plots, as labeled, are 4 milli-Hz, 2 milli-Hz and 0.2 milli-Hz. As labeled in the plot title, the sensed Z4 is averaged for 10 sec, 10 sec, and 5 min respectively from the 500 Hz raw LOWFS data.

3.3 Testbed results: coronagraph dynamic test - demonstrating LOWFS/C to maintain the coronagraph contrast with the presence of WFIRST like disturbances

The LOWFS/C has demonstrated FSM and DM closed-loop performance to suppress the WFIRST-like LoS and low order WFE disturbances and LOWFS testbed data match the control models' predictions. However, the ultimate demonstration of LOWFS/C is to evaluate the LOWFS/C closed-loops performance using the HLC and SPC coronagraphs. The LOWFS/C has to show that it can maintain the high contrast of the coronagraphs and improve the coronagraph contrast stability in presence of the WFIRST-like disturbances. This dynamic demonstration of coronagraph high contrast imaging with LOWFS/C suppressing WFIRST-like disturbances is our last major milestone (Milestone 9 or MS9 for short) for the technology development on the testbed. We have achieved this milestone in Jan of 2017 on our OMC testbed for both the HLC and SPC coronagraphs.

Figure 11 and Figure 12 show the coronagraph dynamic test results. Both figure plot the coronagraph contrast recorded during the dynamic test. Figure 11 is the results from testbed's Hybrid Lyot Coronagraph (HLC) and Figure 12 shows the results from the Shaped Pupil Coronagraph (SPC).

A typical dynamic test, whether using HLC or SPC, follows a test sequence listed below:

(1) The initial step before the dynamic test is to establish a broadband (11% centered at 550 nm) high contrast imaging on coronagraph using the iterative high order wavefront control, often referred as EFC (electric field conjugation) [18, 17]. This is done with the OMC testbed in "static" condition without LoS and low order WFE injection from the OTA Simulator.

(2) The high order wavefront control (EFC) is stopped once a good contrast (about a few $\times 10^{-9}$) has been established. The dynamic test then starts and the OMC's Science Camera begins to continuously monitor the broadband (11% centered at 550 nm) contrast throughout the dynamic test. The Science Camera measures contrast at rate of about one measurement every 7 to 10 sec. The recorded contrast data are plotted in Figure 11 and 12.

(3) The dynamic test starts with a segment of contrast data under "static" the lab environment. Usually we turn on the FSM feedback loop during this period to reduce the LoS drift in the lab environment. In this period, no WFIRST disturbance is injected and the data will provide us a base line on the testbed low order WFE drift.

(4) Use OTA Simulator to inject WFIRST Cycle 5 disturbances into the testbed. The disturbances include: (a) LoS drift of 14 mas (RMS) from ACS with "knee" frequency at 0.2 Hz; (b) LoS jitter from the worst reaction wheel speed at 600 rpm. The LoS jitter contains 72 harmonics beside the fundamental frequency of 10 Hz. The total energy of LoS jitter is about 4 mas (RMS); (c) sinusoidal focus (Z4) disturbance with amplitude of ±0.5 nm (RMS) for HLC dynamic test in Figure 11, or ±1 nm (RMS) for SPC dynamic test in Figure 12, and period of 750 sec (12.5 minutes). The LoS disturbances listed (a) and (b) are generated by OTA Simulator's Jitter Mirror. The sinusoidal focus disturbance is generated by moving the pseudo star pinhole using a linear stage. WFIRST Cycle 5 model shows that the WFIRST thermally induced WFE is about 0.5 nm (RMS) and focus is the dominant term. We use the varying focus error on testbed to represent all the low order WFE WFIRST would suffer. The amount of low order WFE we put in is, therefore, about 2X (HLC test) to 4X (SPC test) that of WFIRST Cycle 5. We also want to point out that, to expedite the experiment, the focus disturbance injected during the dynamic test is about 10X to 20X faster than WFIRST would experience although on the testbed our pseudo star source is much brighter than a real star.

(5) Close LOWFS/C FSM line-of-sight loops and DM focus correction loop with WFIRST-like disturbances injected into the testbed. In the dynamic test we chose to use the DM #2 for low order WFE correction since

the DM #1 has been used to correct testbed static aberrations. The coronagraph contrast results from this period demonstrate the LOWFS/C capability to suppress disturbances to maintain the contrast and contrast stability of the coronagraph. The Milestone 9 requirement is to maintain the 10% broadband contrast to below 10^{-8} during this period and the plots in Figure 11 and 12 have shown just that.

(6) With the WFE disturbances still on, we then turn off the LOWFS/C's DM focus correction loop while keep the LoS feedback and feedforward loops on. This segment's data show the impact of contrast and contrast stability without the low order WFE (focus) correction.

(7) With the WFE disturbances still on, we turn off the LoS feedforward loop in addition to the DM loop (Figure 11). This segment's data show the contrast and contrast stability degradation from the focus drift and LoS jitter.

(8) With the WFE disturbances still on, we turn off the LoS feedback too so that all the correction loops, FSM LoS and DM low order WFE, are off. This segment data show the contrast and contrast stability degradation from WFIRST-like disturbances without any LOWFS/C corrections.

(9) The dynamic test ends with a segment or two of data in which all WFIRST-like disturbances are turned off and testbed is back to the lab environment. Compare this segment with the beginning segment of dynamic test in step (3) we can evaluate the impact of testbed drift.

Legends and captions of Figure 11 and 12 provide more detail descriptions on the test conditions and specifics. Some general observations regarding to the dynamic test results are:

- The LOWFS/C LoS loops using the FSM and low order WFE correction loop using a DM have been demonstrated on both the HLC and SPC coronagraphs. The LOWFS/C has shown to be able to maintain the coronagraph contrast to better than 10^{-8} with presence of WFIRST-like disturbances. Without LOWFS/C, the coronagraph contrast level and contrast stability would be severely degraded and would not be useful for WFIRST coronagraph science.
- The LoS disturbances contribute the most of the contrast degradation. Both LoS drift and LoS jitter need to be sensed and corrected by FSM loops.
- Although the coronagraph contrast degradation from the focus error injected is much less compared to LoS disturbances, the contrast stability has significantly degraded if the focus variation was not suppressed.
- The starting contrast in our dynamic test was worse than the best contrast achieved on the testbed, especially for HLC. This is due to the noises from strain gauges in OTA Simulator's PZTs, especially these on the JM. We need these strain gauges on in order to generate the precise disturbances deigned.
- In the period when all LOWFS/C loops are closed to correct WFIRST disturbances the coronagraph contrast still have small residual variations with the period matching the sinusoidal input of focus disturbances. This residual is mainly caused by the DM actuator gain calibration error. The imperfect knowledge of DM actuator gain will result in fitting errors when a DM is used to correct low order WFE. The DM low order WFE fitting error are of mid to high spatial frequencies where the LOWFS sensor is insensitive. Our previous SPIE paper has studied this effect in details [19].
- There is an underline testbed drift presented. Investigations have shown that the drift is mostly coming from deformable mirrors. DMs are sensitive to the temperature variations, and some of the DM actuators have long settling time.
- The LOWFS/C helps to increase contrast stability even when the testbed is under lab environment because LOWFS/C can correct testbed line-of-sight drift and low order WFE drift. Some of the best contrasts on testbed were achieved with aids of LOWFS/C under lab environment [16].

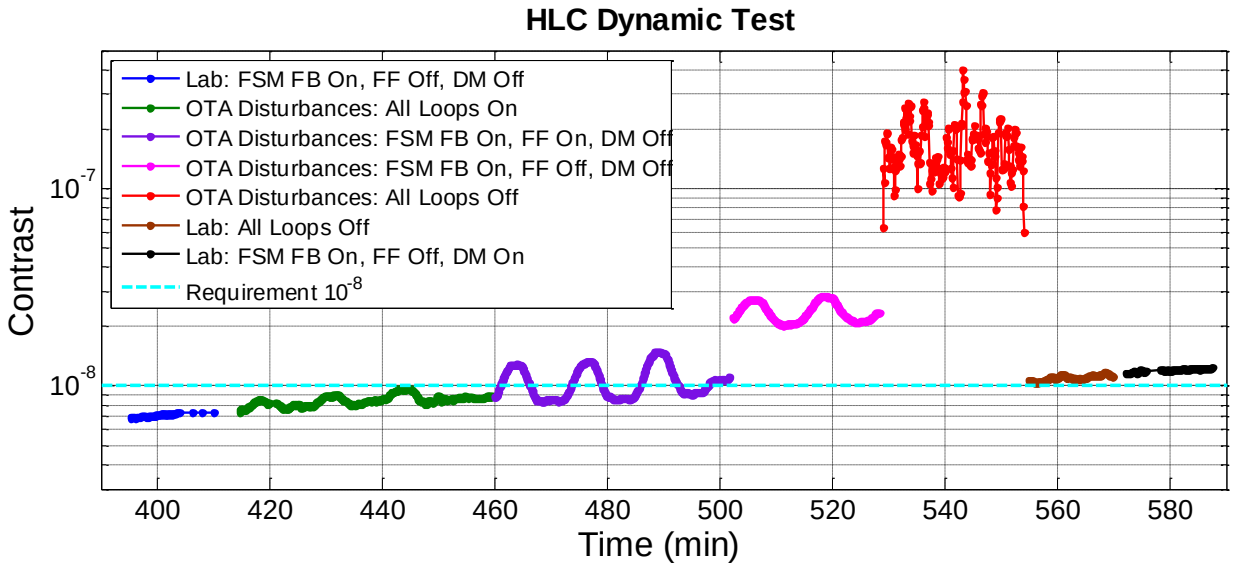

Figure 11. HLC dynamic test results that show the HLC contrast under various dynamic conditions. The plot follows the test sequence with data of each segment plotted in a different color. The Y-axis is the HLC broadband (11% centered at 550 nm) contrast in logarithmic scale and X-axis is time in minutes, which is referenced to an earlier time in this plot. From left to right the test segments are: (1) Blue curve: testbed in the lab environment, no OTA Simulator injected disturbances, FSM feedback loop on, FSM feedforward loop off, and DM low order WFE correction loop off. This segment provided us an initial condition under the lab environment so we could monitor the testbed drift. (2) Green curve: the LOWFS/C dynamic closed loop performance. The OTA Simulator injected WFIRST-like disturbances into testbed and all LOWFS correction loops (FSM & DM) were closed. The injected disturbances were: 14 mas of LoS drift, LoS jitter at RWA wheel speed of 600 rpm, sinusoidal focus error with sinewave amplitude of ±0.5 nm and period of 12.5 minutes. In this segment there were about three sinewave cycles of focus. The post corrected contrast curve mimics the input focus errors. The requirement for the MS9 is to maintain the contrast below 10^{-8}, which is indicated by the cyan dash line. (3) Purple curve: under the same disturbances, the DM focus correction loop was turned off. The HLC contrast responded to the injected sinusoidal focus error. Because the coronagraph contrast goes with the square of wavefront error, we would expect six peaks from the three cycles of focus. However, during this test there was some focus offset in HLC that has skewed the periodic contrast curve. Therefore, we only saw three peaks instead of six. (4) Pink curve: under same disturbances, the DM focus loop and LoS feedforward loop were turned off while the LoS feedback loop was still on. The coronagraph contrast still had the similar response to the focus sinewave like that in segment (3), but the uncompensated LoS jitter has raised the contrast floor higher. We only recorded about two cycles of focus for this segment. Again, we saw only two peaks instead of expected four due to the HLC had some focus offset. (5) Red curve: the testbed was still under the same disturbances but all the FSM LoS and DM low order WFE loops were turned off. The contrast and contrast stability were at the worst level. This underlines the necessary of LOWFS/C for WFIRST CGI. (6) Brown curve: back to lab environment with no OTA Simulator disturbances injection. For this segment, we turned off FSM and DM loops. Compared to segment (1) the contrast had drifted higher. As matter of fact, there was an obvious linear trend of all the minimum contrast level data points for the entire HLC test session. (7) Black curve: testbed under lab environment but FSM feedback loop and DM focus loop were turned on. The underline drift was still going on, but compared to previous segment (6), the FSM and DM loops have helped to smooth out the contrast variations, improving the testbed's short term contrast stability.

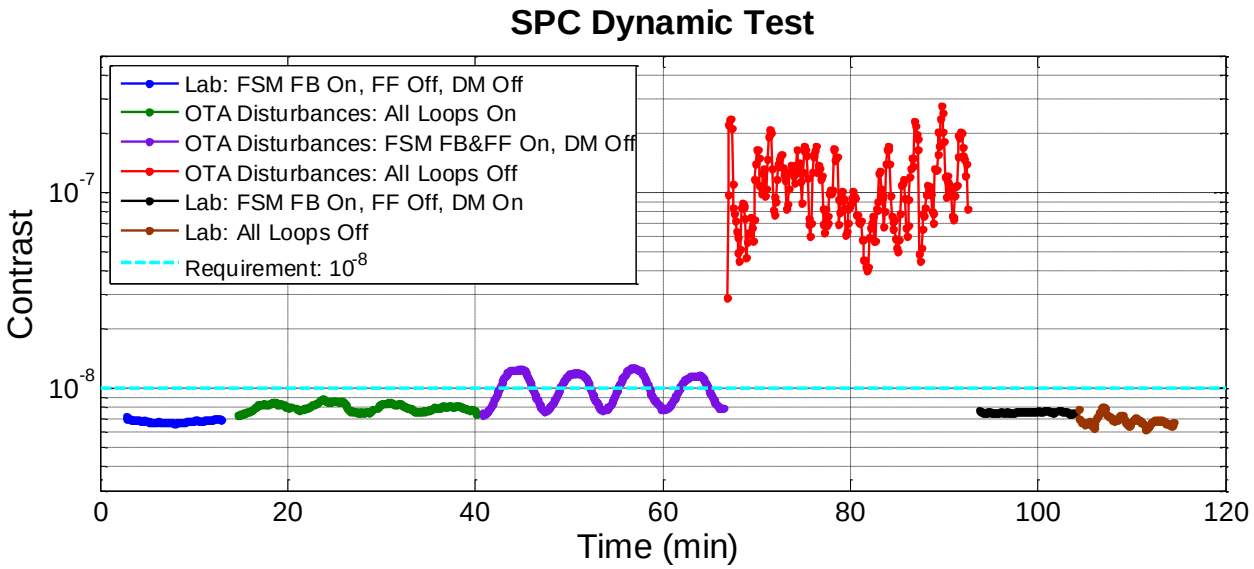

Figure 12. SPC dynamic test results that show the SPC contrast under various dynamic conditions. The plot follows the test sequence with data of each segment plotted in a different color. The Y-axis is the SPC broadband (11% centered at 550 nm) contrast in logarithmic scale and the X-axis is time in minutes. From left to right the test segments are: (1) Blue curve: testbed in the lab environment, no OTA Simulator injected disturbances, FSM feedback loop on, FSM feedforward loop off, and DM low order WFE correction loop off. This data segment provided us an initial condition under the lab environment so we could monitor the testbed drift. (2) Green curve: the LOWFS/C dynamic closed loop performance. The OTA Simulator injected WFIRST-like disturbances into testbed and all LOWFS correction loops (FSM & DM) were closed. The injected disturbances were: 14 mas of LoS drift, LoS jitter at RWA wheel speed of 600 rpm, sinusoidal focus error with sinewave amplitude of ±1 nm and period of 12.5 minutes. This segment contained about two sinewave cycles of focus. The post corrected contrast curve mimics the input focus errors. The requirement for the MS9 is to maintain the contrast below 10^{-8}, which is indicated by the cyan dash line. (3) Purple curve: under the same disturbances, the DM focus correction loop was turned off. The SPC contrast responded to the injected sinusoidal focus error. Because the coronagraph contrast goes with the square of wavefront error, so we observed four peaks from the two sinewave cycles of focus. (4) Red curve: the testbed was still under the same disturbances but all the FSM LoS and DM low order WFE loops were turned off. The contrast and contrast stability were at the worst level. This underlines the necessary of LOWFS/C for WFIRST CGI. (5) Black curve: back to lab environment with no OTA Simulator disturbances injection. For this segment, the FSM feedback loop and DM loop were turned on. Compared to segment (1) the contrast had drifted higher although much less that of HLC test seen in Figure 11. (6) Brown curve: testbed under lab environment. All the LOWFS/C loops were turned off. We can see that compared to segment (5), without any LOWFS/C loops the SPC contrast varied more, even though during this period the testbed drift had favored coronagraph contrast level.

4 CONCLUSION AND FUTURE WORK

The WFIRST coronagraph LOWFS/C subsystem uses the Zernike wavefront sensor, which has the phase shifting disk combined with the coronagraph's focal plane mask, to sense the low order wavefront drift and line-of-sight error using the rejected starlight. The dynamic OMC testbed including Hybrid Lyot Coronagraph, Shaped Pupil Coronagraph, low order wavefront sensor, and the OTA Simulator has been built to demonstrate LOWFS/C performance together with the coronagraphs. The LOWFS sensor has demonstrated high sensitivity, capable of sensing LoS tilt to the level of 0.2 mas and low order mode to the level of 12 pm. The dynamic tests have shown that LOWFS/C can maintain coronagraph contrast to better than 10^{-8} in presence of WFIRST-like LoS and low order WFE disturbances in both SPC and HLC modes. Data from line-of-sight control using the FSM and low order wavefront correction using a DM have matched the control models predictions. LOWFS/C correction greatly improves OMC contrast stability and is beneficial to the coronagraph even when the testbed is under the lab environment.

Coronagraph and LOWFS/C technology developments continue on the OMC testbed. The area we are currently working on are operating the testbed in WFIRST flight like operation configuration including LOWFS/C under low stellar flux. With testbed being improved and evolved, we will further improve the coronagraph performance, algorithm robustness, calibration accuracy, control efficiency, and model agreement. Eventually we will transform the technology development testbed into a WFIRST CGI instrument engineering testbed to test flight hardware and algorithms, and more importantly, support the WFIRST CGI flight instrument I&T.

ACKNOWLEDGMENTS

This research was carried out at the Jet Propulsion Laboratory, California Institute of Technology, under a contract with the National Aeronautics and Space Administration. The work published in this paper was funded by NASA's WFIRST project.

REFERENCES

[1] Demers, R., Dekens, F. G., Calvet, R. J., Chang, Z., Effinger, R. T., Ek, E. M., Jones, L., Loc, A., Nemati, B., Noecker, C., Neville, T., Pham, H., Tang, H., and Villalvazo, J., "Requirements and design reference mission for the WFIRST-AFTA coronagraph instrument," Proc. SPIE **9605**, pp. 9605-1, (2015).

[2] Tang, T., Demers, R., Krist, J., McGuire, J., Rud, M., Zhao, F., "The WFIRST Coronagraph Instrument Optical Design Update," Proc. SPIE **10400**, 10400-02, (2017).

[3] Mandell, A., Groff, T., Rizzo, M., Gong, Q., Zimmerman, N., Harvey, D., Saxena, P., Prada, C. M., Cady, E., "Current science requirements and planned implementation for the WFIRST-CGI Integral Field Spectrograph (IFS)," Proc. SPIE **10400**, 10400-09, (2017).

[4] Krist, J., Nemati, B., and Mennesson, B., "Numerical modelling of the proposed WFIRST-AFTA coronagraphs and their predicted performances," JATIS **2**, (2016).

[5] Krist, J., Riggs, A.J., McGuire, I., Tang, H., Amiri, N., Gutt, G., Marchen, L., Marx, D., Nemati, B., Saini, N., Sidick, E., Zhou, H., "WFIRST coronagraph optical modeling," Proc. SPIE **10400**, 10400-04, (2017).

[6] Balasubramanian, K., White, V., Yee, K., Echternach, P., Muller, R., Dickie, M., Cady, E., Ryan, D., Poberezhskiy, I., Zhao, H., Kern, B., Krist, J., Nemati, B., Patterson, K., Riggs, A.J., Zimmerman, N., and N. J. Kasdin, "WFIRST-AFTA coronagraph shaped pupil masks: Design, Fabrication and Characterization," JATIS **2**, (2016).

[7] Balasubramanian, K., Riggs, A. J., Cady, E., White, V., Yee, K., Wilson, D., Echternarch, P., Muller, R., Prada, C. M., Seo, J., Shi, F., Ryan, D., Fregoso, S., Metzman, J., Wilson, R. C., "Fabrication of WFIRST coronagraph masks and laboratory scale star-shade masks: characteristics, defects, and performance," Proc. SPIE **10400**, 10400-12, (2017).

[8] Zernike, K., MNRAS, **94**, 377, (1934).

[9] Wallace, J. K., Rao, S., Jensen-Clem, R. M., and Serabyn, G., "Phase-Shifting Zernike Interferometer Wavefront Sensor," Proc. SPIE **8126**, (2011).

[10] Shi, F., Balasubramanian, K., Hein, R., Lam, R., Moore, D., Moore, J., Patterson, K., Poberezhskiy, I., Shields, J., Sidick, E., Tang, H., Truong, T., Wallace, J. K., Wang, X., and Wilson, D., "Low Order Wavefront Sensing and Control for WFIRST-AFTA Coronagraph," JATIS **2**, (2016).

[11] Wang, X., Shi, F., and Wallace, J. K., "Zernike wavefront sensor (ZWFS) development for low order wavefront sensing (LOWFS)," Proc. SPIE **9904**-243, (2016).

[12] Shields, J., Shi, F., Lam, R., Truong, T., and Patterson, K., "Narrowband rejection of reaction wheel and environmental disturbances for the WFIRST OMC testbed," Guidance, navigation, and control, Vol 159, pp 251-262, (2017)

[13] Patterson, K., Shields, J., Wang, X., Tang, H., Azizi, A., Brugarolas, P., Mandic, M., and Shi, F., "Control Design for Momentum-Compensated Fast Steering Mirror for the WFIRST-AFTA Coronagraph Instrument," Proc. SPIE **9605**, pp. 9605-83, (2015).

[14] Shi, F., Balasubramanian, K., Bartos, R., Hein, R., Lam, R., Mandic, M., Moore, D., Moore, J., Patterson, K., Poberezhskiy, I., Shields, J., Sidick, E., Tang, H., Truong, T., Wallace, J. K., Wang, X., and Wilson, D., "Low order wavefront sensing and control for WFIRST coronagraph," Proc. SPIE **9904**, 990418, (2016).
[15] Cady, E., Seo, B.-J., Balasubramanian, K., Greer, F., Gordon, B., Kasdin, J., Kern, B., Kuhnert, A., Marx, D., Prada, C. M., Moody, D, Muller, R., Poberezhskiy, I., Riggs, A.J., Trauger, J., Wilson, D., White, V., Yee, K., Zimmerman, N., and Zhou, H., "Milestone 5 Final Report: Hybrid Lyot and Shaped Pupil Broadband Contrast Testbed demonstration for WFIRST-AFTA," https://wfirst.gsfc.nasa.gov/science/sdt_public/wps/references/WFIRST_CGI_Milestone5_Final_Report.pdf.
[16] Cady, E., Balasubramanian, K., Gersh-Range, J., Kasdin, J., Kern, B., Lam, R., Prada, C. M., Moody, D., Patterson, K., Poberezhskiy, I., Riggs, A. J., Seo, B.-J., Shi, F., Tang, H., Trauger, J., Zhou, H., Zimmerman, N., "Shaped pupil coronagraphy for WFIRST: high-contrast broadband testbed demonstration," Proc. SPIE **10400**, 10400-14, (2017).
[17] Seo, B.-J., Cady, E., Gordon, B., Kern, B., Marx, D., Moody, D, Muller, R., Patterson, K., Poberezhskiy, I., Shi, F., Sidick, E., Trauger, J., and Wilson, D., "Hybrid Lyot coronagraph for WFIRST: high-contrast broadband testbed demonstration," Proc. SPIE **10400**, 10400-15, (2017).
[18] Give'on, A., Kern, B., Shaklan, S., Moody, D., and Pueyo, L., "Broadband wavefront correction algorithm for high-contrast imaging system," Proc. SPIE, **6691**, 66910A, (2007).
[19] Sidick, E. and Shi, F., "Effect of DM actuator errors on the WFIRST/AFTA coronagraph contrast performance," Proc. SPIE **9605**, 960506, (2015).